

KfK 4480
November 1988

Inclusive Measurements of the Break-up of 156 MeV ${}^6\text{Li}$ -Ions at Extreme Forward Angles and the Quasi Free Break-up Model

H. Jelitto, J. Buschmann, V. Corcalciuc, H. J. Gils, N. Heide,
J. Kiener, H. Rebel, C. Samanta, S. Zagromski
Institut für Kernphysik

Kernforschungszentrum Karlsruhe

KERNFORSCHUNGSZENTRUM KARLSRUHE

Institut für Kernphysik

KfK 4480

INCLUSIVE MEASUREMENTS OF THE BREAK-UP OF 156 MEV ${}^6\text{Li}$ -IONS
AT EXTREME FORWARD ANGLES
AND THE QUASI FREE BREAK-UP MODEL

H. Jelitto, J. Buschmann, V. Corcalciuc^{*}, H.J. Gils, N. Heide,
J. Kiener, H. Rebel, C. Samanta^{**}, and S. Zagromski

^{*} Central Institute of Physics, IFIN, P.O.B. MG6,
Bucharest-Magurele, Romania

^{**} SAHA Institute of Nuclear Physics, Bidhan Nagar,
Calcutta 700064, India

Kernforschungszentrum Karlsruhe GmbH, Karlsruhe

Als Manuskript vervielfältigt
Für diesen Bericht behalten wir uns alle Rechte vor

Kernforschungszentrum Karlsruhe GmbH
Postfach 3640, 7500 Karlsruhe 1

ISSN 0303-4003

INCLUSIVE MEASUREMENTS OF THE BREAK-UP OF 156 MEV ${}^6\text{Li}$ -IONS AT EXTREME FORWARD ANGLES AND THE QUASI FREE BREAK-UP MODEL

Abstract

Inclusive alpha particle and deuteron spectra from collisions of 156 MeV ${}^6\text{Li}$ -ions with ${}^{12}\text{C}$ and ${}^{208}\text{Pb}$ were measured at extreme forward emission angles including zero degree. The measurements were performed with the Karlsruhe magnetic spectrograph 'Little John' and required an efficient reduction of the background from small-angle scattering. The observed double differential cross sections and angular distributions have been analysed on the basis of Serber's spectator break-up model. When going to angles smaller than grazing, where Coulomb effects are expected to be dominating, transitional features may appear. Corresponding effects probably associated with Coulomb break-up are observed with the ${}^{208}\text{Pb}$ -target and require a slight extension of the Serber approach. In the case of the ${}^{12}\text{C}$ -target the break-up cross sections in forward direction seem to reflect the shape of the internal momentum distribution of the alpha particle and deuteron cluster in the ${}^6\text{Li}$ -projectile and are in agreement with a 2S-type wave function. However, at larger angles the shape appears to be distorted, possibly by final state interactions.

INKLUSIVE MESSUNGEN DES AUFBRUCHS VON 156 MEV ${}^6\text{Li}$ -IONEN UNTER EXTREMEN VORWÄRTSWINKELN UND DAS QUASI-FREIE AUFBRUCH-MODELL

Zusammenfassung

Es wurden inklusive Alphateilchen- und Deuteronen-Spektren aus Stößen von 156 MeV ${}^6\text{Li}$ -Ionen mit ${}^{12}\text{C}$ und ${}^{208}\text{Pb}$ im extremen Vorwärtswinkelbereich einschließlich der Null-Grad-Richtung aufgenommen. Die Messungen wurden mit dem Karlsruher Magnetspektrographen 'Little John' durchgeführt und verlangten eine effektive Unterdrückung des Untergrundes, hervorgerufen durch Vorwärtswinkelstreuung. Die beobachteten doppelt-differentiellen Wirkungsquerschnitte und Winkelverteilungen wurden auf der Basis des Aufbruch-Modells von Serber analysiert. Zu kleineren Winkeln unterhalb des Streifwinkels, wo eine Dominanz von Coulombeffekten erwartet wird, können Übergangsphänomene auftreten. Entsprechende Effekte, die vermutlich auf den Coulomb-Aufbruch zurückzuführen sind, wurden beim ${}^{208}\text{Pb}$ -Target beobachtet und machen eine geringfügige Erweiterung des Serber Ansatzes notwendig. Im Falle des ${}^{12}\text{C}$ -Targets scheinen die Aufbruch-Wirkungsquerschnitte in Vorwärtsrichtung die Form der inneren Impulsverteilung des Alphateilchen- und Deuteronen-Clusters widerzuspiegeln und entsprechen einer 2S-Wellenfunktion. Jedoch zeigen sich bei größeren Streuwinkeln Distortionseffekte, möglicherweise hervorgerufen durch Endzustandswechselwirkungen.

CONTENTS

1. Introduction	1
2. Experimental set-up and procedures	2
3. Data processing	6
4. Experimental results	8
5. Theoretical basis of the analysis	13
6. Comparison of measured results and theory	19
7. Concluding remarks	25
Acknowledgement	27
Appendix A: Distortions affecting the Serber model cross section	28
Appendix B: Energy shifts of the break-up maxima	31
References	34

1. Introduction

The break-up of composite nuclear projectiles in the field of atomic nuclei is an important reaction mode in nucleus-nucleus collisions at high as well as low incident projectile energies [1]. It comprises a large fraction of the total reaction cross section and is often signalled by broad and pronounced bumps centered around the beam-velocity energies in the continuum part of the inclusive energy spectra of the emitted particles. The strongly forward-peaked angular distributions and other features, very distinct in reactions induced by loosely bound projectiles like ${}^6,7\text{Li}$ [2-7], suggest that the bumps dominantly originate from fast peripheral fragmentation processes of the projectile, in which the observed fragment remains a spectator of the reaction [8,9].

Thus, the basic scenario shows a projectile $a = (b + x)$ with the velocity v_a hitting a nucleus A in a grazing collision and a spectator b , which moves on essentially undisturbed. This implies that its velocity after colliding is determined by the projectile velocity superimposed by the Fermi motion. The participant x interacts with the target in a variety of reaction modes, elastically (elastic break-up) or preferably nonelastically [10]. In such break-up reactions the projectile is lifted into the continuum, where it immediately disintegrates and the fragments are assumed not to influence each other any more. In contrast, in another extreme situation the target field excites an intermediate resonance via inelastic scattering or even cluster transfer, which subsequently decays influenced by the final state interaction of the fragments in the 'excited' projectile (sequential or resonant break-up). To which extend one or the other basic mechanism is prevailing in a particular situation and is contributing to the observed inclusive spectra of the break-up fragments is a question of interest.

The most simple spectator model describing the main features of the disintegration of nuclear projectiles was introduced by Serber [8]. It is based on a pure geometric approach in momentum space, equivalent to a plane wave description in r -space, thus implying minimum distortion by the nuclear target field. Treating the target nucleus as a black disk includes absorption of the unobserved fragment x ('opaque model'). Coulomb effects like the deflection and the deceleration of the projectile in the Coulomb field of the target are included on the basis of quasi-classical considerations.

In general, the quasi free approach disregards the distortion of the incoming and outgoing waves. This deficiency is removed by the very successful (post-form) DWBA-approach worked out by Baur et al. [10,11]. However, due to a zero-range approximation, necessary for practical calculations, the DWBA-approach implies a constraint of the squared projectile wave function $|\tilde{\phi}_a(\mathbf{q})|^2$ to a Lorentzian distribution. An additional numerical problem arises from the large number of partial waves to be considered at very small emission angles when

including the Coulomb break-up. The use of the PWBA-expressions appears to be more flexible in this respect.

In the past, quasi free break-up approaches (spectator models) have been discussed with data of fragment emission close to or larger than the grazing angle, i.e. resulting from processes dominantly induced by the nuclear interaction in the periphery of the target nucleus. When observing at emission angles considerably smaller than grazing the influence of the Coulomb interaction from larger impact parameters is of increasing importance, and a change in the character of the break-up process is expected. The aim of the present work is to look experimentally for corresponding transitional features.

For this purpose inclusive alpha particle and deuteron spectra from the collision of 156 MeV ${}^6\text{Li}$ -projectiles with ${}^{12}\text{C}$ and ${}^{208}\text{Pb}$ have been measured at extreme forward angles. The experiment takes profit of the magnetic spectrograph 'Little John'. It extends available data, which were previously measured with semiconductor telescopes [4] and were limited to an angular region $\geq 10^\circ$, to smaller angles including 0° . Due to the well-developed cluster structure of ${}^6\text{Li}$ showing very distinct break-up phenomena, ${}^6\text{Li}$ -projectiles are considered to be most suitable for the intended studies. The experimental results are discussed on the basis of an extended version of the Serber model including a component of small Coulomb deflection angles. The analysis provides an insight into the character of the break-up reaction mechanisms at very forward emission angles.

2. Experimental set-up and procedures

The measurements were performed at the Karlsruhe Isochronous Cyclotron using ${}^6\text{Li}^{3+}$ -particles from the external ECR ion source LISKA [12,13]. The ${}^6\text{Li}$ -particles were axially injected into the cyclotron and accelerated to a beam energy of 156 MeV. The charged particle spectra were measured with the magnetic spectrograph 'Little John' (Fig. 1), which has a QQDS-magnet configuration and is particularly designed for the detection in extreme forward direction [14,15]. It is equipped with a focal plane detector [15,16], which can be moved along the direction of the particle trajectories for a variable momentum acceptance and resolution, respectively. This requires a flexible imaging of the system which is performed by the quadrupole doublet (QQ). The sextupole magnet (S) enables to adjust the focal plane to be perpendicular to the central trajectory. A mode with a large momentum acceptance ($\pm 9.1\%$) and low resolution was used in this case, where the vacuum extensions VE2 and VE3 were removed (see Fig. 1).

The focal plane detector consists of two position sensitive proportional counters providing the momentum information by measuring the position in the focal plane via charge division

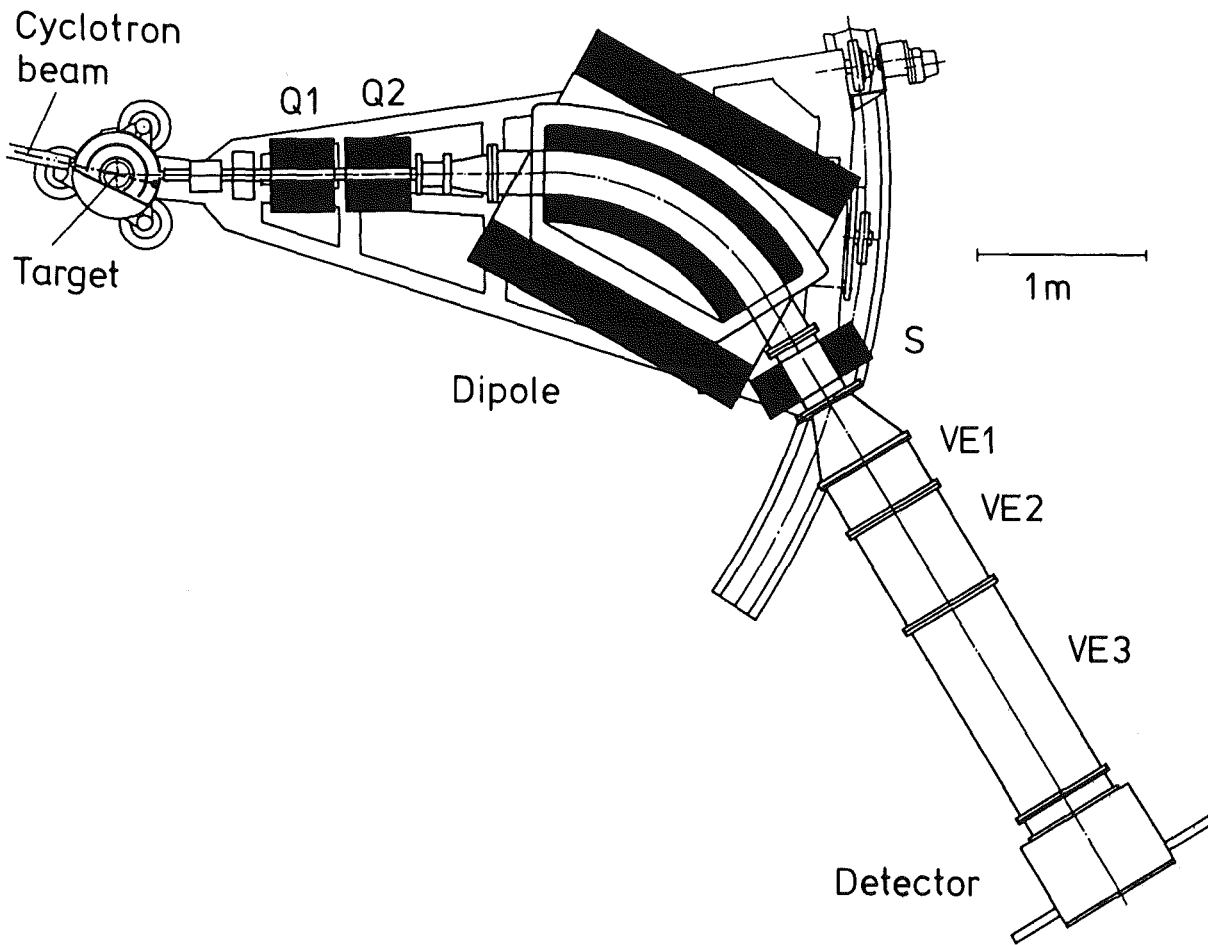


Fig. 1: The Karlsruhe Magnetic Spectrograph 'Little John'.

at a thin wire. An additional ionisation chamber and a plastic scintillator, measuring the energy loss ΔE and the remaining energy E , are used for particle identification. These four single detectors, each of which has an efficiency for particle detection close to 100 % [16,17], were operated in coincidence to reduce neutron and gamma induced background.

At small observation angles several characteristic problems arise caused by the 'beam halo', the angular straggling from the target and the high counting rate from elastic ${}^6\text{Li}$ -scattering, which is up to five orders of magnitude larger than the break-up contribution. The beam halo was minimised by a very careful preparation of the primary beam using emittance reducing slits in the extraction system of the cyclotron and upstream the monochromator magnet, and using anti-scattering diaphragms downstream in the beam line

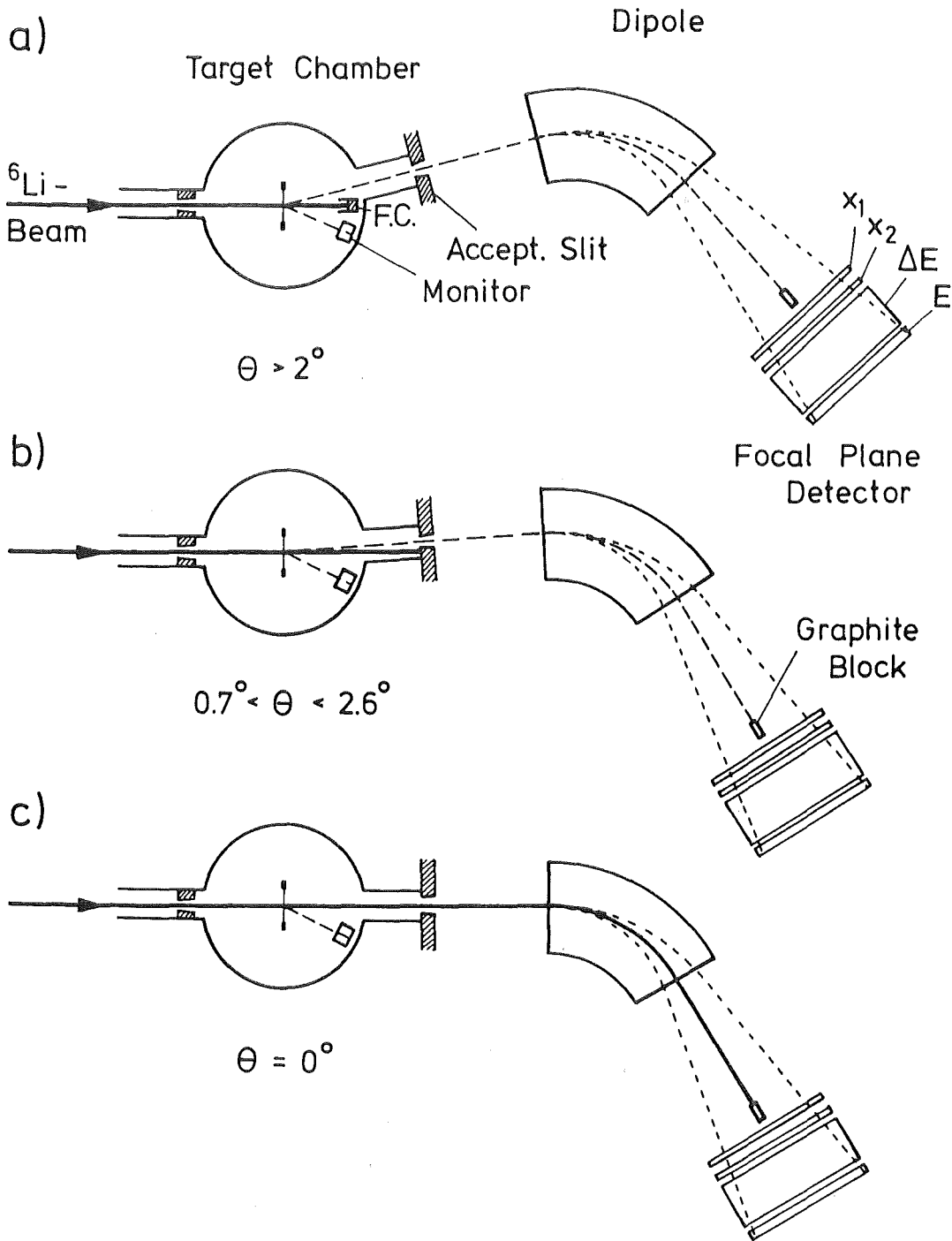


Fig. 2: Mechanical set-ups (schematically drawn) to stop the primary beam for measurements in different angular ranges.

[16,18]. The beam spot on the target had a diameter of about 1 mm. At the beginning of each experiment an angular beam profile was measured, which had an average width of 0.10° and allowed to determine the 0° -direction within an accuracy of better than $\pm 0.05^\circ$. The beam current was limited by the counting rate in the detector to values between 5 nA and 50 pA for reaction angles 10° down to 0.7° and to about 1 pA at 0° .

The angular range in forward direction was covered by three different set-ups for stopping the primary beam as illustrated in Fig. 2. Dependent on the observation angle the ${}^6\text{Li}$ -beam was stopped either in a Faraday cup inside the 50 cm ϕ target chamber or on a graphite block, which is fixed on the acceptance diaphragm. For the zero degree measurement the beamstop was a small 20 mm broad carbon block placed in front of the focal plane detector. This beamstop produced a comparatively narrow gap in the energy spectra and could only be used when particles with $Z > 1$ were to be detected.

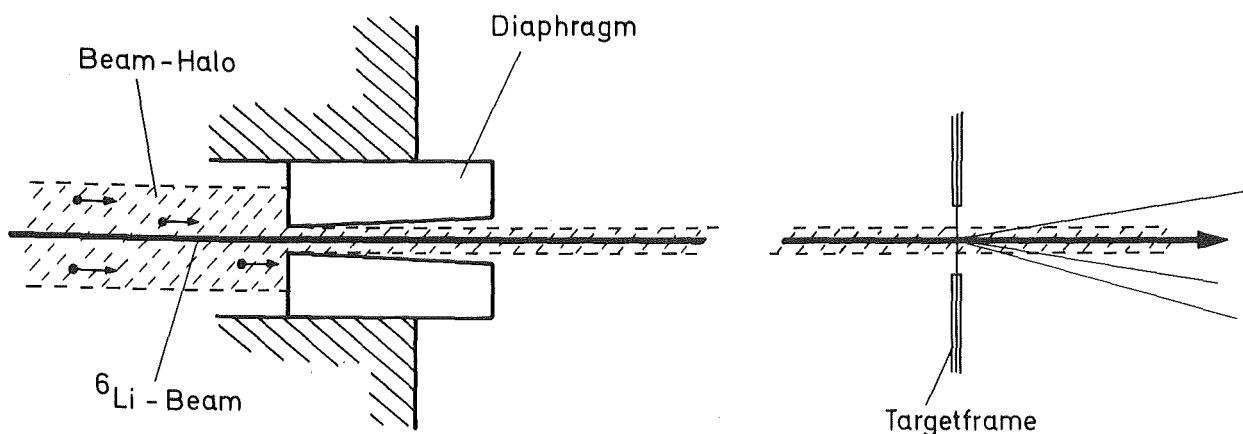


Fig. 3: The entrance of the target chamber with a diaphragm to reduce remaining ${}^6\text{Li}$ -particles from the beam halo (idealised).

In order to prevent ${}^6\text{Li}$ -particles of the remaining beam halo from hitting the target frame and enlarging the number of background events a 7 mm ϕ conical diaphragm was positioned at the entrance of the target chamber (Fig. 3). In combination with a large target frame of 15 mm diameter a measurement with a blank target indicated that nearly no background remained from beam halo particles at forward angles. This method was considerably

improved later on with active suppression systems [16,19] which are necessary when detecting ${}^6\text{Li}$ -ejectiles (for instance for giant resonance measurements [19]).

The break-up alpha particles and deuterons have about beam velocity and the charge-to-mass ratios of alpha particles, deuterons and ${}^6\text{Li}$ are the same. This means that the elastically scattered ${}^6\text{Li}$ -particles and the maxima of the break-up alpha particle and deuteron spectra are positioned at approximately the same horizontal place in the focal plane. Therefore, the carbon block for stopping the primary beam at 0° was also used to stop the elastically scattered ${}^6\text{Li}$ -particles at positive angles. Thus, a small energy gap is created as a peculiarity of all measured spectra, but it reduces the overall counting rate in the focal plane detector by nearly two orders of magnitude. In this angular range a width of 10 mm for the graphite block turns out to be sufficient. (In an early state of the experiment the block with 20 mm width was also used for 1° and 2° , see Fig. 9, ${}^{12}\text{C}$ -target.) Since the gap is at a known energy it provides an additional control of the energy calibration.

For absolute normalisation of the cross sections at angles larger than 2° the beam current on the Faraday cup in the target chamber was integrated. An additional gas counter [20] in the target chamber positioned at $\Theta = -17^\circ$ at a distance of 60 mm from the target allowed an exact relative normalisation of the spectra at different observation angles. The measurement of the beam current with the beam stop on the acceptance diaphragm was rather inaccurate, because here the escape of secondary electrons was not suppressed. Therefore, the gas detector was indispensable for normalisation from 2° down to 0° .

3. Data processing

A separation of the different particle types can be performed very easily using the energy loss and total energy information by setting particle specific windows in a two-dimensional ΔE - E -diagram, where the different ejectiles are clearly separated [16].

An accurate energy calibration over the whole momentum acceptance of the spectrograph is very important since continuous particle spectra not containing clear peaks at well known energies are to be measured and the shape of the spectrum yields essential physical information. Furthermore, due to higher-order ion-optical properties and detector nonlinearities the momentum of the particles is not a linear function of the calculated position in the focal plane.

The primary data were recorded event by event on magnetic tape (list mode) each containing six 12-bit words using a data acquisition program [19] on a PDP 11/23 computer. The data reduction comprises two main steps. At first 'position spectra' were created, cal-

culating the apparent position x of a particle in the focal plane with $x = K \cdot Q_L / (Q_L + Q_R)$, where Q_L and Q_R are charge signals from the left and right side of the wire in the position sensitive detectors and K is the maximum channel number in the spectrum. Test measurements indicated [17] that electrical off-sets P_L and P_R of the charge signals largely influence the resolution of the spectra. This requires to replace Q_L by $Q_L' = Q_L - P_L$ in the given expression and to replace Q_R analogously. Secondly, the position spectra were converted into energy spectra for which an energy calibration is needed. It was performed by placing the peak of elastically scattered ${}^6\text{Li}$ -particles on five equidistant positions in the focal plane varying the magnetic field. The calculated positions were used to determine a polynomial of 4th degree representing the momentum and the energy, respectively, as a function of the calculated position K , involving nonlinearities of the detector and the ion-optics of the spectrograph simultaneously. The procedure and especially the influence of different particle types and different magnetic settings is described in detail in refs. [16,18].

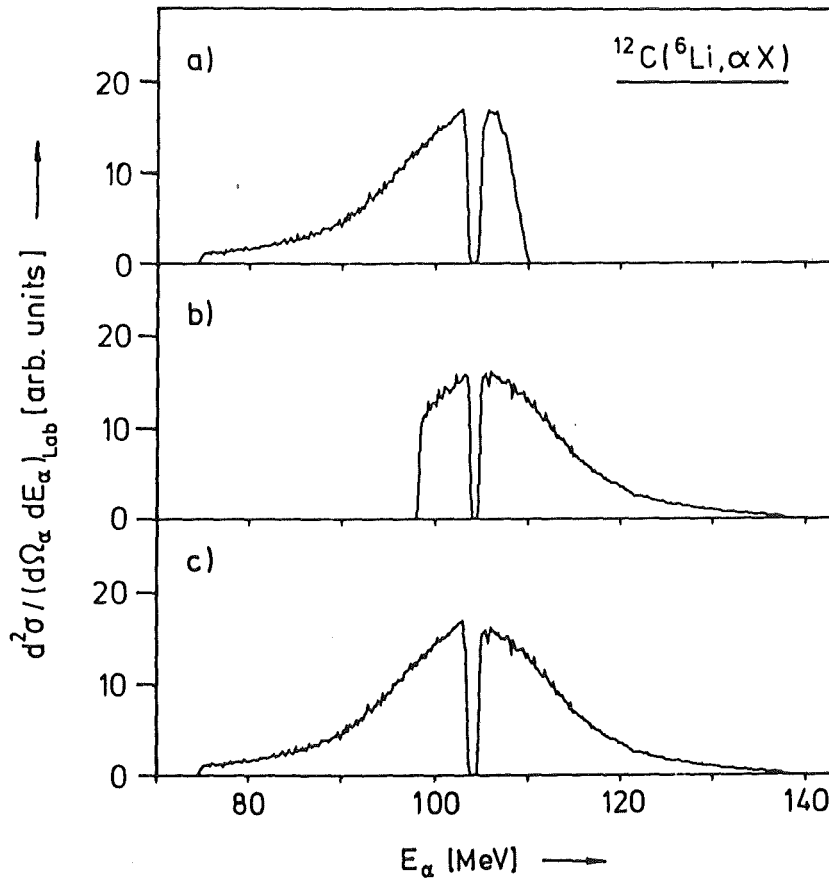


Fig. 4: Inclusive alpha particle spectra of the reaction ${}^6\text{Li} + {}^{12}\text{C}$ at $\Theta_{\text{lab}} = 2^\circ$ with two different magnetic settings (a, b) and the combined spectrum (c).

The covered energy range, which is 39 MeV for alpha particles and 19.5 MeV for deuterons, can be enlarged by measuring with different magnetic settings and combining the partial energy spectra. An example of a combined inclusive energy spectrum is displayed in Fig. 4. This spectrum also shows that the preequilibrium background is small compared to the break-up component in the forward angular range. Yet the main measurements (Fig. 5,6) were performed with only one magnetic setting in order to exclude inaccuracies for this first experiment, possibly originating from an insufficient accuracy of the magnetic field measurement.

4. Experimental results

Inclusive alpha particles and deuterons from the break-up of 156 MeV ${}^6\text{Li}$ -projectiles when bombarding ${}^{12}\text{C}$ and ${}^{208}\text{Pb}$ -targets were detected for emission angles from 12° down to 0° . Table 1 contains details of the selfsupporting target foils.

Table 1: Target properties

Target	Enrichment [%]	Thickness [mg/cm^2]
${}^{12}\text{C}$	98.98	4.3
${}^{208}\text{Pb}$	> 99	8.1

A series of alpha particle spectra in the observed angular range is shown in Fig. 5. The gap in the middle of each spectrum originates from the carbon block, which was used to suppress the elastic line. (When using the ${}^{208}\text{Pb}$ -target the 0° -Spectrum exhibits an experimental background below beam velocity energy, probably due to the angular straggling in the target with secondary scattering of ${}^6\text{Li}$ -ions at the acceptance diaphragm, and is therefore not used.) The physical background, mainly due to preequilibrium and equilibrium processes, decreases with increasing energy and is small compared to the break-up contribution at forward angles.

In the previous experiments of Neumann et al. [4] this background contribution was approximated by a straight line. In our case this procedure leads to additional uncertainty because the covered energy range is limited. Neumann et al. found that the physical background is independent of the observation angles between 10° and 32° . It can be assumed that this background contribution remains constant for angles down to 0° . Thus, the background estimate [21] was taken from alpha particle and deuteron spectra at the emission angle 12° , which is also covered in this experiment. The background is represented by the

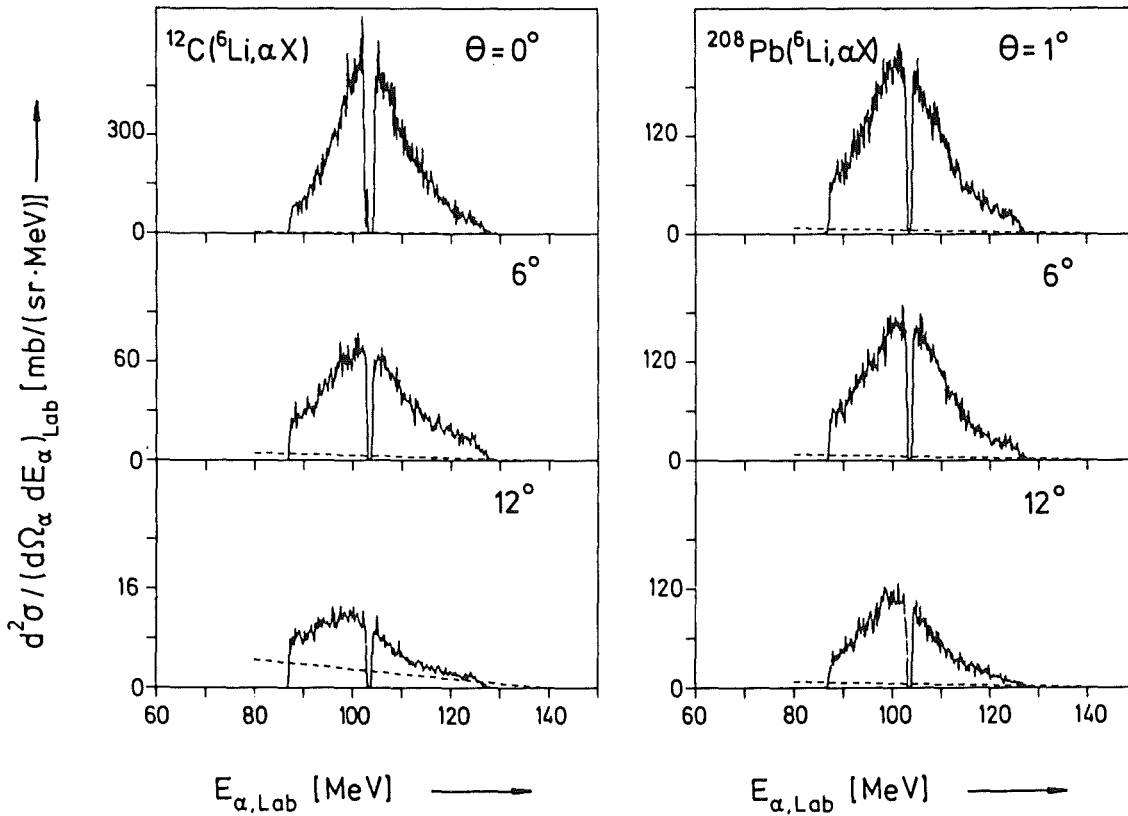


Fig. 5: Inclusive alpha particle spectra from collisions of 156 MeV ^6Li -ions with ^{12}C and ^{208}Pb in the forward angular range. The physical background represented by the dashed lines is taken from [21].

dashed lines in Fig. 5 and is subtracted later on when comparing the break-up spectra with model predictions (Figs. 9,10,13).

In order to obtain the angular distributions by integrating the break-up contributions of the energy spectra a different way of considering the background was chosen for practical purposes. For alpha particle spectra it was shown by comparison with data from [21] that the measured physical background and the amount of break-up particles, which is outside the expected energy range of the actual setting of the spectrograph, in average cancel each other. Therefore, the energy spectra were integrated without any background subtraction. The maximum error of this procedure is estimated to be less than 10% and even decreases towards smaller angles [18]. The different energy windows for alpha particles and deuterons

were taken into account by an additional factor 1.6 in the angular distribution of the break-up deuterons, which was determined by comparing the acquired areas of the break-up bumps from alpha particles and deuterons [18].

The measured energy integrated cross sections can be compared directly with the corresponding data from Neumann et al. [4] in the overlapping angular region of 10° to 12° . The latter cross sections are smaller for the ^{12}C -target by 23% and for the ^{208}Pb -target by 12%. This is a reasonable agreement taking into account e.g. the error in measuring the target thicknesses. Finally, our data were normalised to those of Neumann et al.. The resulting break-up angular distributions are displayed in Fig. 6.. Additionally, the measured cross sections of the elastic ^6Li -scattering divided by the Rutherford cross sections are represented by the upper data points.

The total break-up cross sections in ref. [4] were calculated by adjusting a function $\sigma(\Theta) = C \cdot e^{-a\Theta}$ (Θ = laboratory angle) to the angular distributions and integrating over the 4π solid angle. In the present experiment especially the angular distribution of alpha particles from $^{208}\text{Pb}(^6\text{Li},\alpha X)$ showed up to be much more flat, than it was extrapolated to small angles with the above assumption. Therefore, another function was adjusted in the forward angular range using the same exponential expression with different parameters. The parameters from [4] were used for the remaining solid angle. The integral production cross sections σ_{int} and the parameters are listed in Table 2.

Table 2: Break-up cross sections and related quantities

Target	Ejectile	Angular range (Θ)	C [b]	a	σ_{int} [b]
^{208}Pb	α	$\leq 12.1^\circ$	4.0	2.1	0.71
		$> 12.1^\circ$	63.4*	15.2*	
^{208}Pb	d	$\leq 7.3^\circ$	6.6	8.6	0.67
		$> 7.3^\circ$	5.5*	7.2*	
^{12}C	α	$\leq 10.6^\circ$	9.5	17.8	0.20
		$> 10.6^\circ$	5.2*	14.4*	
^{12}C	d	$\leq 7.0^\circ$	3.8	12.8	0.23
		$> 7.0^\circ$	2.1*	7.8*	

* parameters from Neumann et al. [4]

Looking more closely to the positions of the maxima of the energy spectra, they appear to be conspicuously shifted from beam velocity energies towards smaller energies. When

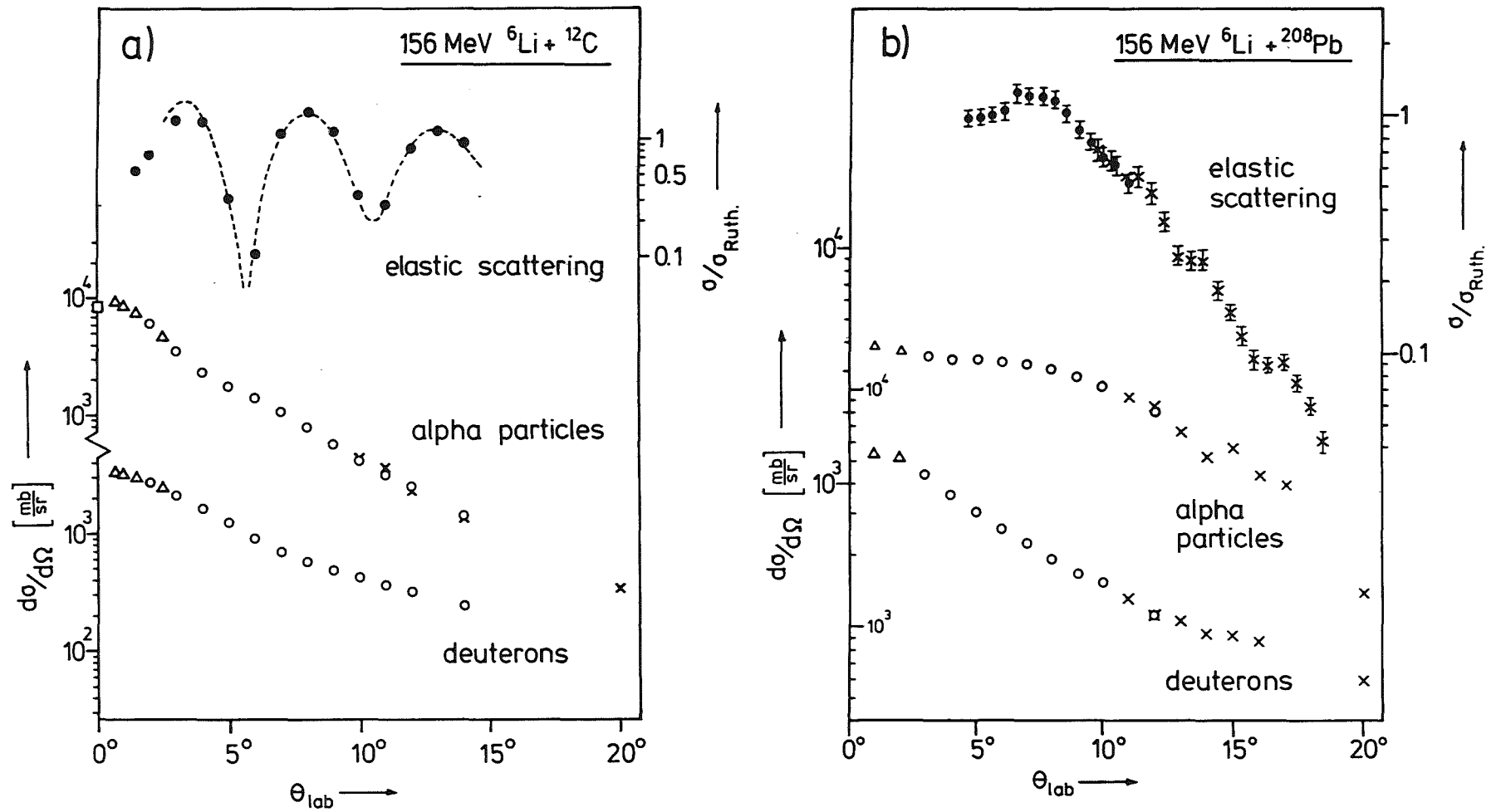


Fig. 6: Measured angular distributions of alpha particle and deuteron fragments from the bombardement of ^{12}C and ^{208}Pb with 156 MeV ^{6}Li -ions. The circles, triangles and the square correspond to the different mechanical set-ups shown in Fig. 2, crosses are data points from ref. [4]. For comparison elastic scattering results are included (with optical model predictions [22] for the ^{12}C case). Crosses in the elastic scattering cross sections (^{208}Pb -target) are from ref. [22].

bombarding ^{12}C -nuclei the shift of the alpha particle spectra increases with increasing emission angle to about 6 MeV at $\Theta_{\text{lab}} = 12^\circ$. When using the ^{208}Pb -target the shifts in the alpha particle spectra are approximately constant with about 2 MeV below 8° and are slightly increasing at larger emission angles. A qualitative explanation of this feature as a geometrical effect is given in Appendix B.

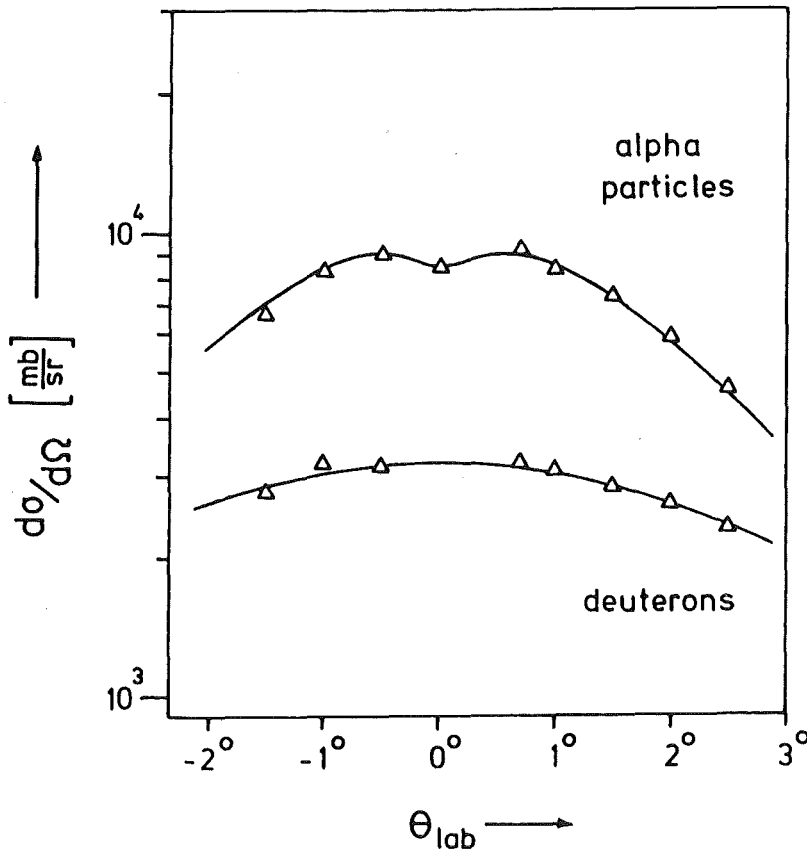


Fig. 7: Angular distribution of break-up fragments from the reaction $^6\text{Li} + ^{12}\text{C}$ at emission angles around 0° . The curves are to guide the eyes.

In principle, an asymmetry of the angular distribution with respect to 0° is possibly due to an asymmetric experimental background, which could be produced for example by the analysing magnet in the beam line. The angular distribution of break-up fragments from the reaction $^6\text{Li} + ^{12}\text{C}$ for emission angles between -1.5° and 2.5° indicate that no asymmetry is observed (Fig. 7).

5. Theoretical basis of the analysis

Although the Serber model approach [8] of projectile break-up reactions is based on a series of simplifying assumptions, it has been proven to be quite useful for exploring the essential features of the physical process underlying the observed phenomena.

The main assumptions are the following: The projectile a consists of two clusters b and x , each with the extension zero and the separation r_{bx} , whereas the target nucleus is treated as a circular disc perpendicular to the beam direction. The energy of the Fermi motion in the projectile should be small compared to the incident energy, which is fairly well fulfilled in the present experiment.

In the most simple form the target is assumed to be transparent to the break-up fragments. Assuming a Yukawa type wave function $\phi(r_{bx})$ for the relative motion of the clusters the double differential cross section in the frame of this 'transparent' (tr.) Serber model (associated with elastic break-up) is given [23] by

$$\frac{d^2\sigma_o^{tr.}}{d\Omega_b dE_b} \propto \rho_{Phase} |\tilde{\phi}(q)|^2 \propto m_b p_b \frac{(2\mu\epsilon)^{1/2}}{(2\mu\epsilon + q^2)^2} \quad (5.1)$$

with the reduced mass μ and the binding energy ϵ of the fragments. The subscript 'o' means, as also in the following, 'without Coulomb effects'. Here the internal momentum q is related to the observed ejectile momentum p_b , the momentum p_{b0} due to the projectile motion and to the emission angle Θ by $q^2 = p_0^2 + p_{b0}^2 - 2p_0 p_{b0} \cos\Theta$.

Actually, the α -d cluster structure of ${}^6\text{Li}$ is hardly described by a Yukawa type wave function. Fig. 8 compares the Yukawa form with the more realistic 2S-type wave function given by Kukulin et al. [24]. In the region of small wave numbers $k < 0.5 \text{ fm}^{-1}$ the momentum distribution can be simulated by a Lorentzian shape using a modified value $\epsilon = 1.07 \text{ MeV}$ (Fig. 8), which is a useful simplification for the extended model described below.

Considering the absorption of the participant fragment by the target nucleus (opaque nucleus), in particular through break-up fusion type processes [3,25,26], leads to the 'opaque' Serber model (superscript 'op.'), where the double differential cross section in eq. 5.1 is modified (calculated by Utsunomiya [23]) to:

$$\frac{d^2\sigma_o^{op.}}{d\Omega_b dE_b} \propto \frac{d^2\sigma_o^{tr.}}{d\Omega_b dE_b} \cdot G(E_b, q, \theta) \quad (5.2)$$

$$G = \frac{(2\mu\varepsilon + q^2)^{1/4} P_{1/2}(s)}{(2\mu\varepsilon + q^2 - p_b^2 \sin^2 \theta)^{3/4}}, \quad (5.2a)$$

and $P_{1/2}(s)$ is a Legendre function of the argument

$$s = \frac{2\mu\varepsilon + q^2 - \frac{1}{2} p_b^2 \sin^2 \theta}{(2\mu\varepsilon + q^2)^{1/2} (2\mu\varepsilon + q^2 - p_b^2 \sin^2 \theta)^{1/2}} \quad (5.2b)$$

The factor G reduces the width of the energy distributions of the break-up fragments and shifts the maxima slightly to larger energies, increasingly with increasing emission angle. The angular distributions of the break-up fragments (explicitly taking into account clusters of different mass) are given by:

$$\frac{d\sigma_o}{d\Omega}(\theta) = \frac{R_T R_{Li}}{\pi(1 + \zeta^2)^{3/2}} \frac{1}{\theta_o^2} C(\zeta) \quad (5.3)$$

with
$$\zeta = \theta/\theta_o, \quad \theta_o = \left(\frac{m_x}{m_b} \frac{\varepsilon}{E_a} \right)^{1/2} \quad (5.3a)$$

and
$$C(\zeta) = \begin{cases} 1 & (\text{transparent model}) \\ 1 - 1/(2\zeta^3) [(1 + \zeta^2) \tan^{-1} \zeta - \zeta] & (\text{opaque model}). \end{cases} \quad (5.3b)$$

The quotient m_x/m_b effects that the angular distribution of the deuterons is more flat than those of the alpha particles. In order to get equal total numbers of both fragment types the factor $1/\theta_o^2$ in eq. 5.3 realises the relative normalisation. (In the original article from Serber this factor is already contained in the solid angle $d\Omega_\zeta$). The parameters R_T and R_{Li} are the target radius and the average separation of the clusters in the ${}^6\text{Li}$ -projectile and provide the absolute normalisation. They are given by Serber only for the opaque model implying a total stripping cross section of $\sigma^{OP} = (\pi/2) \cdot R_{Li} R_T$ (which is also valid when including the Coulomb deflection). This normalisation is simply taken for the transparent model, too, in order to have a definite normalisation for both versions of the model which is necessary for the extension introduced subsequently.

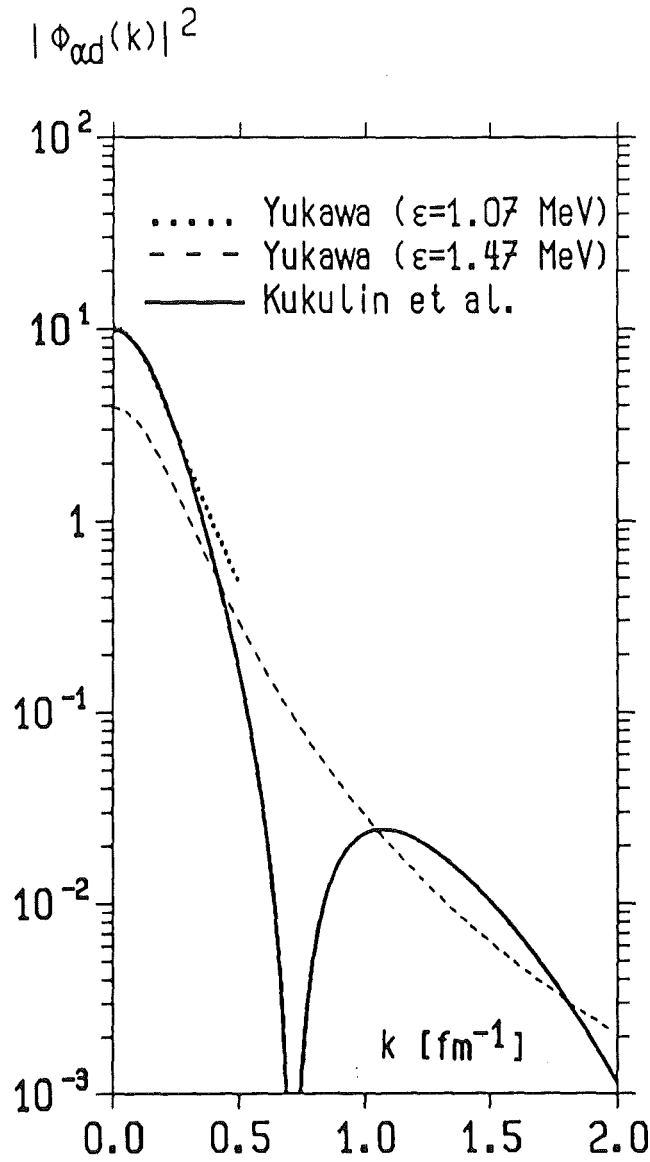


Fig. 8: Various forms of the α -d internal momentum distribution of ${}^6\text{Li}$.

For the target radius the equivalent radius R_e was taken, related to the root mean square radius by $R_e^2 = 5/3 \langle r \rangle^2$. With values for $\langle r \rangle$ taken from [27,28] the target radii are 2.70 fm for ${}^{12}\text{C}$ and 7.32 fm for ${}^{208}\text{Pb}$. If we assume the intrinsic cluster wave function of ${}^6\text{Li}$ to be of Yukawa type, the separation is $R_{\text{Li}} = 1/(2a)$ with $a = (2\mu\epsilon)^{1/2}/\hbar$. (For the Pb-Target one obtains $\sigma^{\text{OP}} = 220$ mb with the modified value $\epsilon = 1.07$ MeV.)

Coulomb interaction effects distort the shape of the angular distributions:

- (i) Due to the Coulomb deceleration the local projectile energy is reduced, when the projectile breaks up. In eq. 5.3a E_a has to be corrected to $E_a - Z_a V_c$, where V_c is the Coulomb energy per unit projectile charge. This leads to a slightly larger width of the angular distribution. Additionally, the Coulomb deceleration of the projectile and the Coulomb acceleration of the break-up fragments afterwards may also shift the positions of the maxima in the energy spectra, away from the beam velocity energies, if the charge-to-mass ratios of projectile and fragments differ. This is not the case for the ${}^6\text{Li} \rightarrow (\alpha + d)$ break-up.
- (ii) The deflection by the transversal momentum from the Fermi motion is superimposed by the deflection of the projectiles due to the repulsive Coulomb field (see also Appendix A). Taking into account the Coulomb repulsion of the projectile and of the observed fragment, the resulting deflection angle is

$$\theta_c = \frac{Z_a V_c}{2E_a} \left[1 + \frac{m_a}{m_b} \frac{Z_b}{Z_a} \right] \cdot K \quad (5.4)$$

with nuclear masses m and charge numbers Z . The factor K is a kinematical factor accounting for the transformation from the c.m. system of projectile and target to the laboratory system. It is 0.67 for ${}^{12}\text{C}$ and 0.97 for ${}^{208}\text{Pb}$ in the range of small angles.

With these effects included the expression of the angular distribution (eq. 5.3) changes to

$$\frac{d\sigma}{d\Omega}(\theta, \theta_c) = \frac{R_T R_{Li} u^{3/2} P_{1/2}(u)}{\pi(1 + \zeta^2 + \zeta_c^2)^{3/2}} \frac{1}{\theta_o^2} C(Q) , \quad (5.5)$$

$$\text{with } u = \frac{1 + \zeta^2 + \zeta_c^2}{\left[(1 + \zeta^2 + \zeta_c^2)^2 - 4\zeta^2\zeta_c^2 \right]^{1/2}} \quad \text{and} \quad \zeta_c = \theta_c / \theta_o . \quad (5.5a)$$

The comparison of the experimental results with the predictions of the standard Serber model approach (through eqs. 5.1 - 5.5) shows that the shapes of the energy distributions are reproduced quite well using an arbitrary normalisation. The angular distributions for the ${}^{208}\text{Pb}$ case, however, suggest that the assumptions of a single average deflection angle Θ_c does not describe well the results for very forward angles, most likely arising from (elastic)

Coulomb break-up at large impact parameters. Therefore we extend the expressions of the standard model by introducing a further component dominating for small angles and large Z_T . This integral term is generated by a superposition of contributions from various deflection angles $\Theta_c' < \Theta_c$. Taking the angular distribution from eq. 5.5 it is extended to

$$\frac{d\sigma}{d\Omega}(\theta, \theta_c) = N \left[\frac{d\sigma^{op/tr.}}{d\Omega}(\theta, \theta_c) + \alpha \int_0^{\theta_c} w(\theta_c') \frac{d\sigma^{tr.}}{d\Omega}(\theta, \theta_c') d\theta_c' \right] \quad (5.6)$$

Here, $w(\Theta_c')$ is an adequate weight function, which is phenomenologically approximated by $w(\Theta_c') = \Theta_c'^n$. While the second term in equation 5.6 proves to be essential for the results with ^{208}Pb -target, it is of little importance in the case of ^{12}C , where Coulomb effects are small.

The contributions with different deflection angles are added incoherently which is a restriction neglecting interference effects. Nevertheless this is in agreement with a work of Akhieser et al. [29]. Within the frame of a diffractive model it is said that in case of an absolutely black target nucleus (Pb-target and alpha particle cluster) there is no interference between diffractive disintegration (nuclear break-up) and disintegration due to the Coulomb interaction (also in agreement with the experiment).

Following these considerations the energy spectra corresponding to equation 5.6 can be obtained when replacing the terms of the angular distributions on the right side of eq. 5.6 by the double differential cross sections (eqs. 5.1 or 5.2) each combined with a factor for the proper relative normalisation:

$$\frac{d^2\sigma^{op/tr.}}{d\Omega_b dE_b}(\theta, \theta_c, E_b) = \frac{d\sigma^{op/tr.}/d\Omega_b(\theta, \theta_c)}{d\sigma_o^{op/tr.}/d\Omega_b(\theta - \theta_c)} \cdot \frac{d^2\sigma_o^{op/tr.}}{d\Omega_b dE_b}(\theta - \theta_c, E_b) \quad (5.7)$$

Thus, the shapes of the energy spectra at the observation angle Θ are given by eqs. 5.1 and 5.2, respectively, evaluated at $(\Theta - \Theta_c)$ and properly normalised to the angular distributions with the Coulomb correction included. Additionally, the double differential cross sections on the right side of eq. 5.7 have to be normalised to the corresponding angular distributions (eqs. 5.3 and 5.5), because of the missing absolute normalisation in eqs. 5.1 and 5.2.

With the background to associate a part or all of the small deflection angles to large impact parameters, which implies Coulomb break-up, an estimate of this part is of interest.

The differential cross section in the integral term of eq. 5.6, integrated over the 4π solid angle, is nearly independent from Θ_c' . Therefore, carrying out the integration in eq. 5.6 and integrating over all scattering angles yields $\sigma^{tr} \cdot \Theta_c^{n+1}/(n+1)$, with the exponent n from the weight function and σ^{tr} being the integrated cross section (transparent model) of eq. 5.3. If we associate only a part of the integral to the Coulomb break-up, namely from $\Theta_c' = 0^0$ up to some 'separation angle' Θ_s , the ratio of this small deflection angle part σ_{sd} to the total break-up contribution for a given ejectile is

$$\frac{\sigma_{sd.}}{\sigma_{tot.}} = \theta_s^{n+1} \left[\frac{(n+1) \sigma^{op./tr.}}{\alpha \sigma^{tr.}} + \theta_c^{n+1} \right]^{-1} \quad (5.8)$$

with Θ_c , α and n being the parameters from eq. 5.6. The integrated cross sections σ^{OP} and σ^{tr} were added, because σ^{tr} is about 25% larger than σ^{OP} , which is a consequence of using the same normalisation factor for both versions of the model (in eqs. 5.3 and 5.5).

6. Comparison of measured results and theory

While the results with ^{12}C represent the case, where the Coulomb field is of minor influence, but target recoil effects show up, the situation with ^{208}Pb appears to be just reversed. Inclusive energy spectra and angular distributions of the break-up fragments from ^6Li collisions with ^{12}C and ^{208}Pb for emission angles from 0° to 12° are displayed in Figs. 9-11. The physical background shown in Fig. 5 is subtracted.

Considering the ^{12}C data the energy spectra (Fig. 9) seem to be best described with the 2S-type momentum distribution at very small angles, whereas the Lorentzian shape (equivalent to a 1S-type cluster wave function) is favoured at $\Theta_\alpha > 3^\circ$ ($\Theta_d > 6^\circ$). The 2S-wave function yields better results with the transparent model at forward angles, whereas the opaque model proves to be superior at $\Theta_\alpha > 3^\circ$. Anticipating that the 2S-type distribution provides the more correct description of the cluster motion in ^6Li [24,30], our observation may indicate that distortion effects around forward direction are negligible and get increasing importance at somewhat larger angles or larger relative momenta \mathbf{q} , respectively. This is supported by $^6\text{Li}(e,e'd)^4\text{He}$ experiments [31] naturally combined with less distortion effects than hadronic reactions. Whereas the measured α -d momentum distribution from ref. [31] is in reasonable agreement up to $\Theta_\alpha = 8^\circ$ with the calculated angular distribution using the 2S-wave function (Fig. 11a), the present alpha particle angular distribution deviates already above 3° . The fact that the 1S-wave function reproduces the measured cross sections in this angular range seems to be in this respect an accidental conformity. When using the exact 2S-wave function [24] (Fig. 11a) the Coulomb deflection, which has very little influence for the ^{12}C -target, is neglected for an easier calculation. Thus, the squared 2S-wave function $|\tilde{\varphi}(\mathbf{q})|^2$ is integrated along q_z for each observation angle as done by Serber. (q_z is the component of \mathbf{q} parallel to the beam direction).

The ratio of measured break-up alpha particles and deuterons, fixed by one common normalisation factor, is well reproduced (Fig. 11a) confirming that nearly an equal number of alpha particles and deuterons originate from ^6Li break-up. This is also corroborated by the almost equal total break-up cross sections for both fragment types given in Table 2. The 'average' scattering angle Θ_0 , as a measure for the width of the angular distributions, adopts values of about 4° for alpha particles and 8° for deuterons, respectively (eq. 5.3a with the separation energy of 1.47 MeV). The lower deuteron yield around 0° is just a consequence of the larger width $\Theta_0(d)$.

Fig. 9 displays also energy spectra of alpha particle ejectiles from ^6Li collisions with ^{208}Pb as compared with the prediction of the extended Serber model. In this case Coulomb effects play a significant role and were taken into account explicitly. The extended model

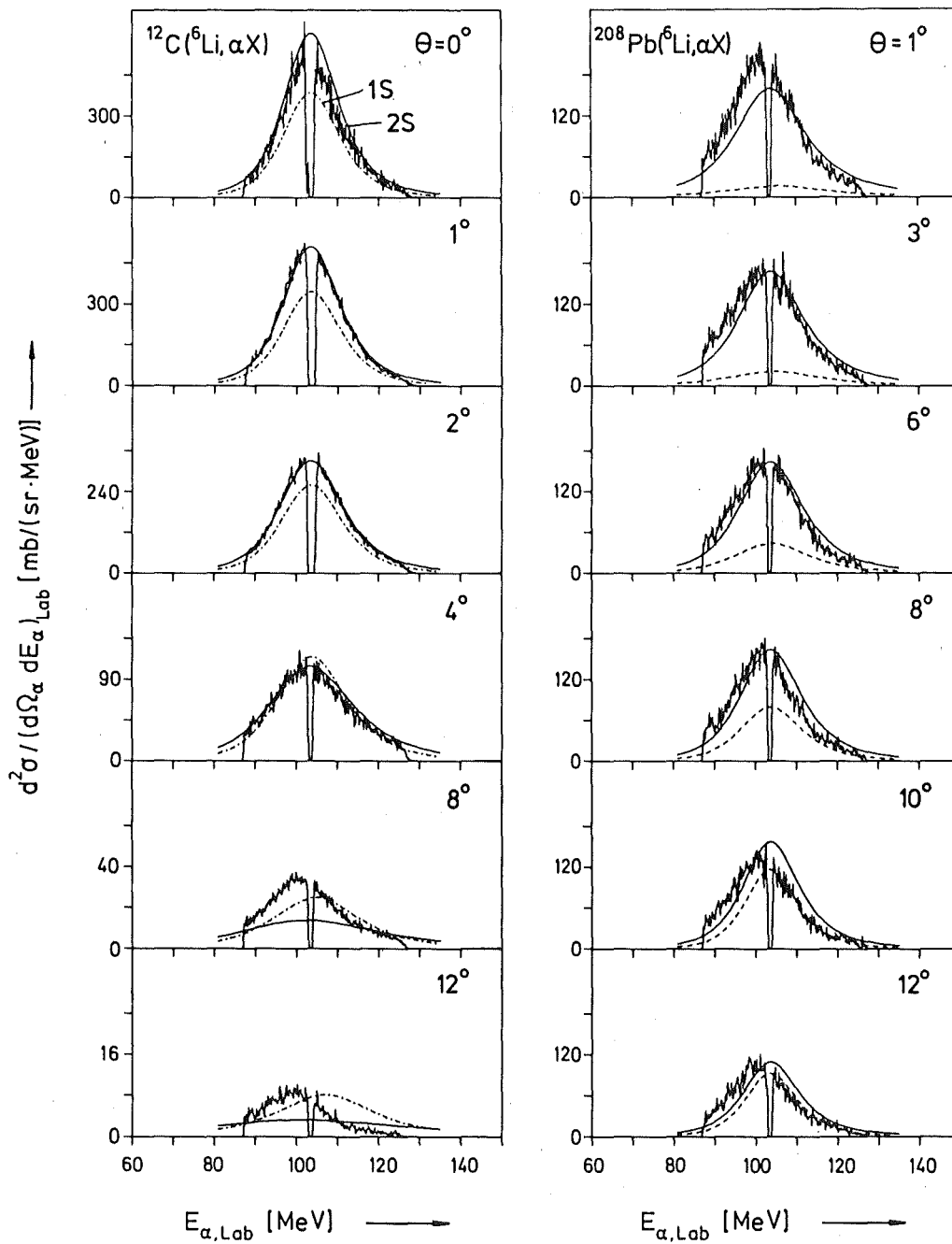


Fig. 9: Experimental and calculated spectra of break-up alpha particles for emission angles between 0° and 12° (with subtraction of the physical background shown in Fig. 5).

- ^{12}C : ——— 2S-wave function (1S with $\epsilon = 1.07$ MeV) and the transparent model,
 - - - - - 1S-wave function and the opaque model.
- ^{208}Pb : ——— extended Serber model,
 - - - - - 'nuclear' break-up contribution ($\Theta_c' \geq 9^\circ$).

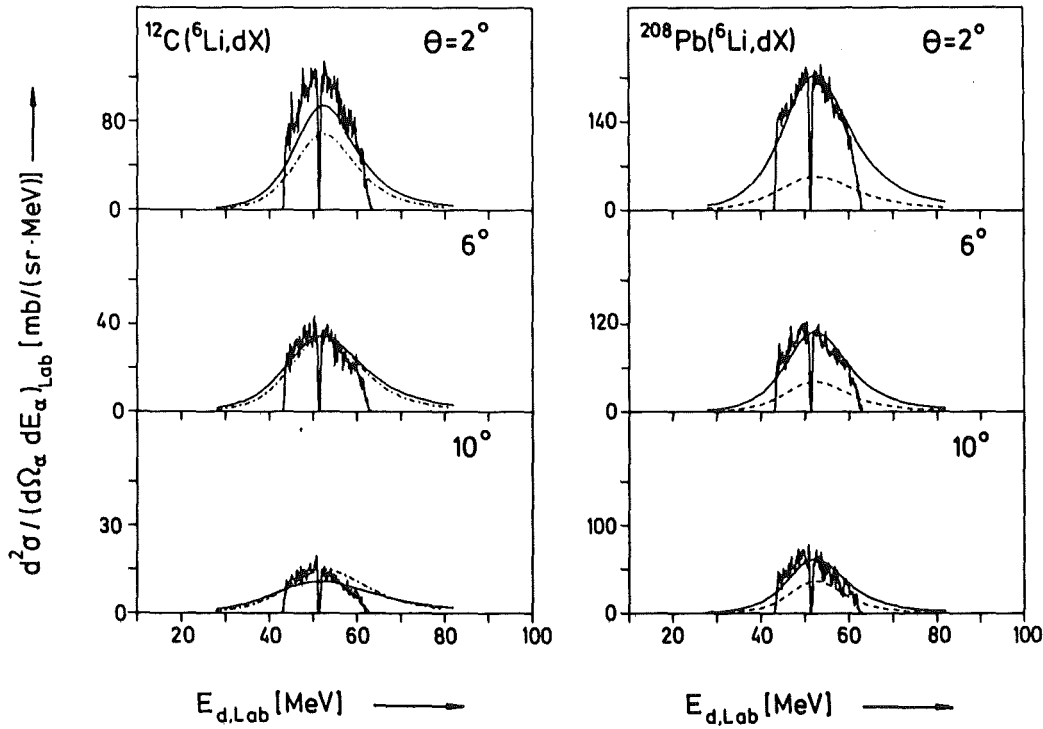


Fig. 10: Experimental energy spectra of break-up deuterons with background subtraction (taken from [21]) and the calculated cross sections as in Fig. 9. For ^{208}Pb the curves are normalised separately for each angle to the experimental data.

reproduces much better the shape and the relative height of the spectra than without the extension.

For comparison some deuteron spectra together with the corresponding theoretical curves are shown in Fig. 10. Because of the deuteron excess at forward angles using the ^{208}Pb -target, which is discussed further on, the absolute heights of the extended model predictions are adjusted separately (one factor for both curves at each emission angle).

In the elastic scattering of the reaction $^6\text{Li} + ^{208}\text{Pb}$ (Fig. 11b) towards smaller angles a transition from scattering in the nuclear field of the target to pure Rutherford scattering can be seen at the small interference maximum at 7° , belonging to the Coulomb rainbow angle. Corresponding interference effects in the angular distributions of the break-up fragments were not observed. Nevertheless, when going from larger angles to forward angle emission below 10° a clear change in the exponential slope of the alpha particle angular distribution

can be seen in Fig. 11b. It can be understood by the deflection of projectile and fragments in the Coulomb field of the target nucleus.

The description of the angular distributions of break-up fragments using the ^{208}Pb -target is based on eq. 5.6 including the small deflection angle part. The value of the deflection angle calculated from eqs. 5.4 is $\Theta_c = 14^\circ$, while a fit of the alpha particle angular distribution to the observed data yields a slightly smaller value $\Theta_c = 11.2^\circ$. This is not surprising as also deflection angles smaller than the maximum value obviously contribute and in average to a smaller mean value.

The improvement of the theoretical description by the second term in eq. 5.6 is obvious from the inspection of the calculated results shown in Fig. 11b. The exponent n of the weight function $w(\Theta_c) = \Theta_c^{-n}$ is adjusted to the data to $n = 0.8$. Table 3 compiles the results of the analysis from both targets on the basis of eq. 5.6, where for ^{208}Pb the alpha particle angular distribution was taken.

Table 3: Parameters of the extended Serber model description.

Target	ϕ_a	Model	Θ_c	N	σ [rad $^{-(n+1)}$]	n
^{208}Pb	$2S^*$	(extend.)	11.2°	0.98	51	0.8
^{12}C	2S	(transp.)	0.0°	2.00^*	0	-
^{12}C	1S	(opaque)	1.0°	2.75	0	-

* approximated by the 1S-function with $\epsilon = 1.07$ MeV

To get an idea of the amount due to (elastic) Coulomb break-up the extended model allows to separate the contribution of small deflection angles. When taking the whole integral term in eq. 5.6 by using eq. 5.8 with $\Theta_s = \Theta_c$ (11.2°) this part comprises 65% of the total break-up cross section for the production of alpha particles (with $\sigma^{\text{op}}/\sigma^{\text{tr}} = 0.8$). The rainbow angle at the small maximum of the elastic cross section is about 7° indicating that the nuclear interaction still contributes at deflection angles smaller than 11.2° . Integration from 0° to $\Theta_s = 7^\circ$ yields an amount of 28% for the 'Coulomb' part. So the amount of the small deflection angle part, probably related to Coulomb break-up, is of the order of one half of the total break-up cross section. Exact predictions are of course not possible, since these numbers stem only from comparison with the extended Serber model. The model predictions are illustrated by the dashed lines in Figs. 9 - 12, where a medium separation angle of $\Theta_s = 9^\circ$ was taken (implying a part of 44% from small deflection angles). The difference between the dashed and the continuous lines can be seen as a measure for the

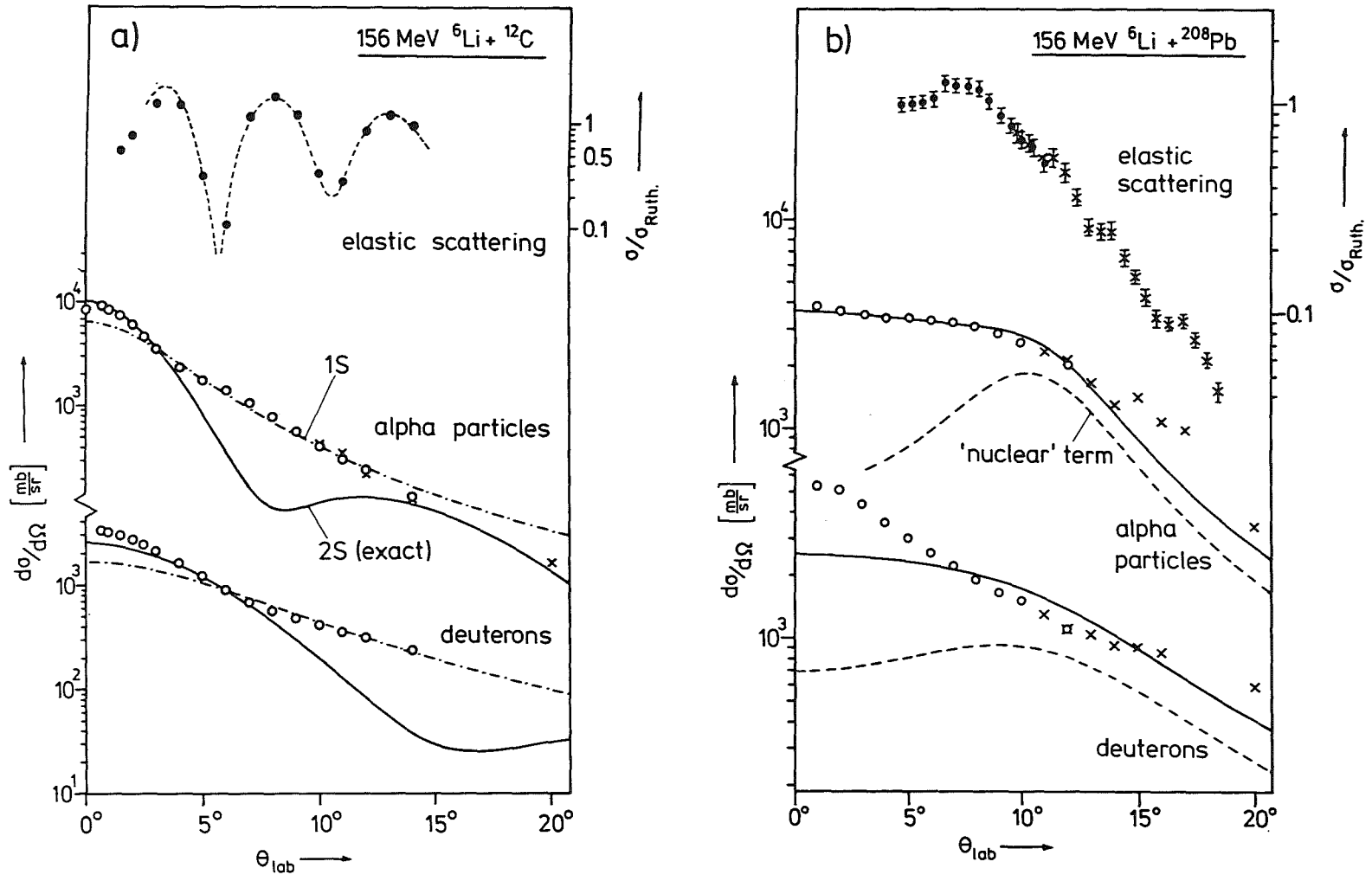


Fig. 11: Angular distributions of alpha particle and deuteron yields from the break-up of 156 MeV ${}^6\text{Li}$ -ions colliding with ${}^{12}\text{C}$ and ${}^{208}\text{Pb}$. a) ——— 2S-wave function and the transparent model, - - - - - 1S-wave function and the opaque model. b) ——— extended Serber model, - - - - - 'nuclear' break-up contribution ($\theta_c' \geq 9^\circ$).

'Coulomb break-up'. In how far this share of small deflection angles really belongs to Coulomb break-up is not yet clear and remains a question for further studies.

The influence of n to the shape of the alpha particle angular distribution is demonstrated in Fig. 12 by using three different values of n . In each case the nuclear break-up cross sec-

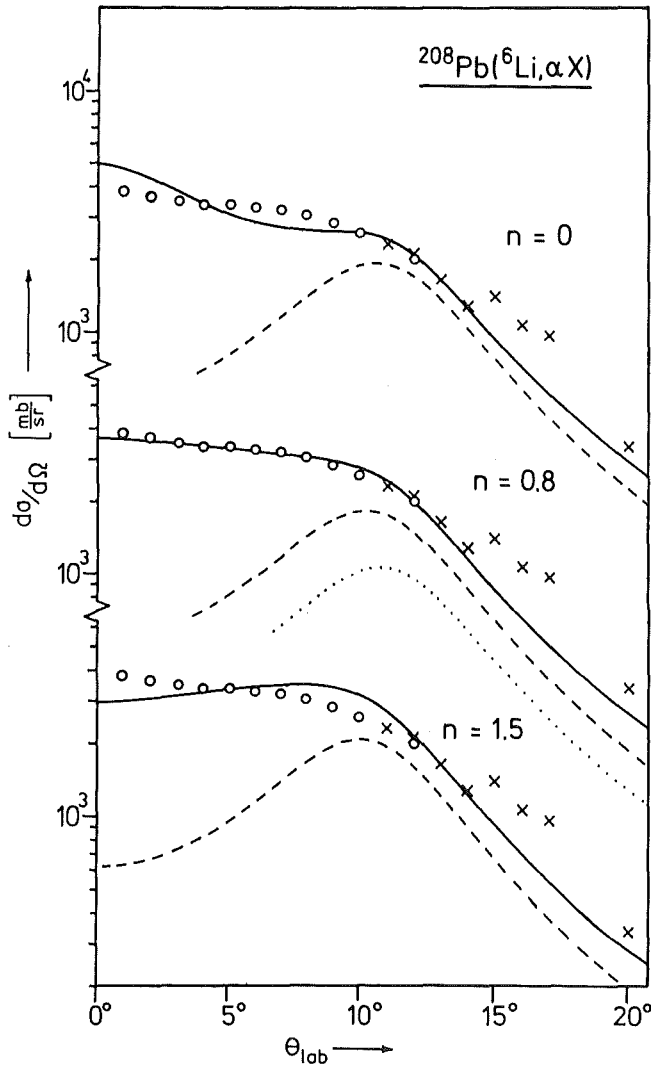


Fig. 12: Calculated angular distributions of break-up alpha particles from the collisions of ${}^6\text{Li}$ with ${}^{208}\text{Pb}$ using different parameters n of the weight function in eq. 5.6. In each case the dashed curves represent the 'nuclear' contribution with $\Theta_c' \geq 9^\circ$. The dotted line shows the contribution from the first term in eq. 5.6 representing the original Serber approach.

tions (large deflection angles and small impact parameters, respectively), represented by the dashed lines, are obtained by integrating up to $\Theta_s = 9^\circ$. It should be noted that the exponent $n = 0.8$ yields the normalisation factor N nearest to 1. (The corresponding normalisation factors N as in Table 3 for the exponents $n = 0$ and $n = 1.5$ are 1.50 and 0.82 with parameters a of 3.6 rad^{-1} and $326 \text{ rad}^{-2.5}$, respectively.) Additionally, the contribution of the first term in eq. 5.6 (opaque model) with one fixed deflection angle is given by the dotted line, which represents the angular distribution from the original Serber approach.

The angular distribution of the deuteron yields from the ^{208}Pb -target (Fig. 11b) is less satisfactorily reproduced. A comparison of the cross sections shows that at emission angles smaller than about 4.5° (classically equivalent to minimum distances larger than ca. 30 fm), more deuterons than alpha particles were measured. This cannot be explained by break-up reactions at large impact parameters, because of the stability of the alpha particle compared to that of the deuteron. This feature has been already observed in previous investigations of ^6Li break-up [2] (when bombarding ^{197}Au with 75 MeV ^6Li). For a tentative explanation this deuteron excess around 0° may not be associated to large angular momenta, rather to small impact parameters in the region of the attractive nuclear force. Due to the reduced absorption of the deuterons [32] as compared to alpha particles the deuterons have a better chance to escape from the nuclear field [4] and to contribute to the forward angle emission.

7. Concluding remarks

Inclusive measurements of projectile fragments from ^6Li -induced nuclear reactions observed at very forward emission angles provide an improved insight into the character of projectile break-up phenomena.

In a rather compressed representation Fig. 13 shows a three-dimensional plot of the experimental cross sections of $^{12}\text{C}(^6\text{Li},\alpha X)$ reactions (including the spectra in Fig. 9) compared with results of the Serber model description. In this case, characterised by a small Z of the target and negligible Coulomb effects, the energy spectra and angular distributions in forward direction mainly reflect the internal momentum distribution due to the Fermi motion in the ^6Li -projectile. In agreement with previous studies [24,30,31] the experimental data seem to be adequately reproduced by the Fourier transformed of a 2S-type cluster wave function, but possibly distorted at larger emission angles by post acceleration effects and final state interactions (see Appendix A).

In the case of ^6Li collisions with ^{208}Pb the Coulomb interaction clearly influences the emission of alpha particle and deuteron fragments. Introducing an additional component for the break-up with Coulomb deflection angles smaller than the mean value, the model pred-

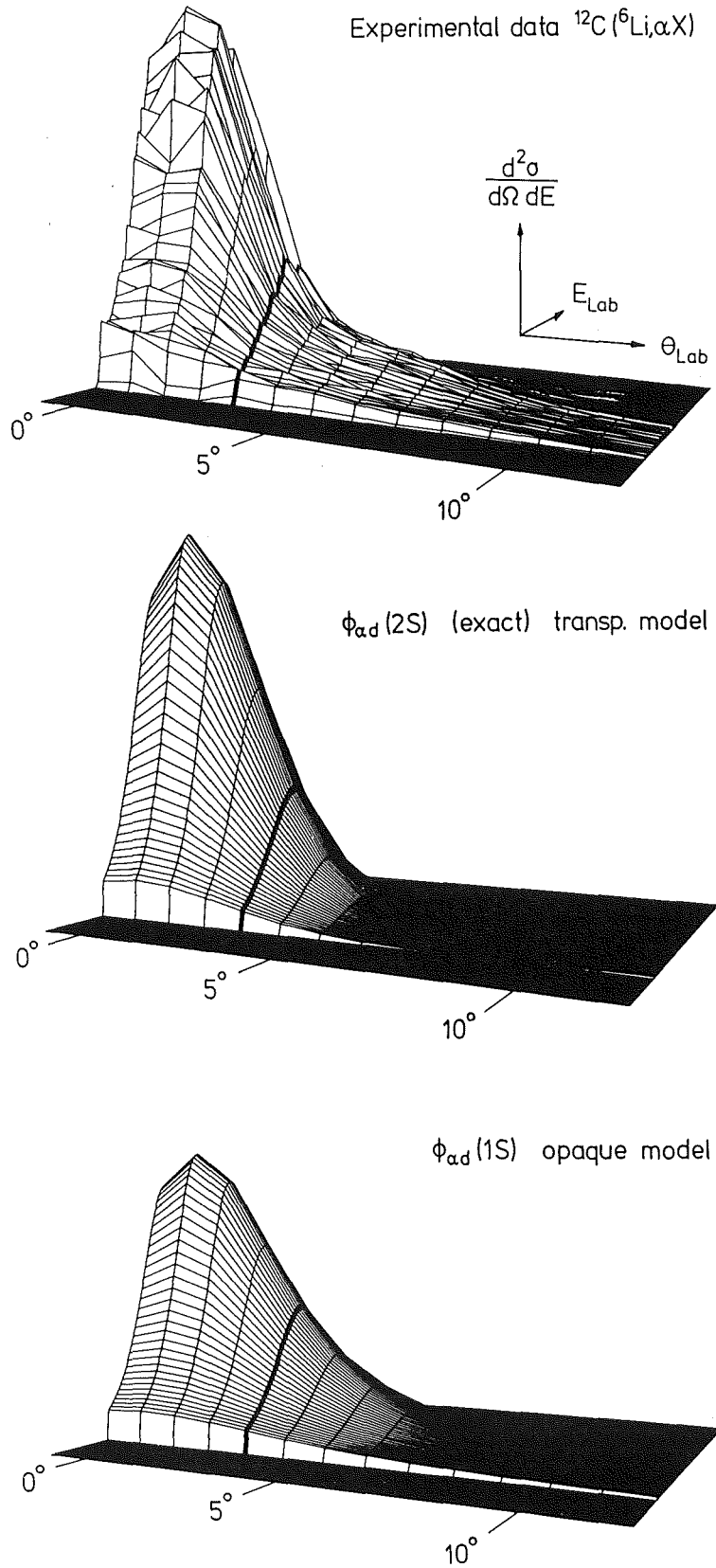


Fig. 13:
Three-dimensional representation of the double differential cross section (linear scale) for the alpha particle emission from collisions of 156 MeV ${}^6\text{Li}$ -ions with ${}^{12}\text{C}$. The energy spectra at 3° (curves set off) are adjusted to equal maximum value (according to the results in Fig. 11a). For the units of the double differential cross section and of E_{lab} compare with Fig. 9.

ictions describe fairly well the experimental data. This extended spectator model naturally separates the break-up contributions from small and large deflection angles, which is an additional information for the discussion about the Coulomb break-up (related to small deflection angles). Of course, an improved analysis should invoke the DWBA-approach [18], for example in the successful post-interaction form worked out by Baur et al. [11]. However, the necessary zero-range approximation constrains the internal momentum distribution to a Lorentzian shape. In addition the large number of partial waves, necessary for the Coulomb break-up at forward angles, makes extensive calculations difficult and perhaps unfeasible.

In the context of the present studies the Karlsruhe magnetic spectrograph 'Little John' [15] has been brought into operation, and the experimental techniques for measurements of the type described here have been worked out. Thus, the results show also that this instrument is well suited for nuclear reaction studies in the extreme forward angle hemisphere, including zero degree.

We thank Prof. Dr. G. Schatz for his continuous interest in our studies and the cyclotron and ion source operation crew, in particular Dipl. Ing. F. Schulz, for their efforts in providing the ${}^6\text{Li}$ -beam. We are also indebted to Prof. Dr. A. Hofmann and Dr. W. Eyrich and their group for valuable help in clarifying some technical problems and especially to Dr. H. Schlösser for providing the used on-line data acquisition computer program. Two of us (V.C. and C.S.) acknowledge the support from the International Bureau (project no. 052.4) and from the Kernforschungszentrum Karlsruhe, and the hospitality received in Karlsruhe while participating in the experiments.

Appendix A. Distortions affecting the Serber model cross section

The Serber model [8] which has been invoked for describing the main features of projectile fragmentation is a particular, highly simplified version of the quasifree break-up approach [9]. Quasifree break-up models (QFBM) are based on a plane wave approximation, thus implying minimum distortion by the target field and ignoring mutual interactions of the fragments in the final state. Following a sequence of approximations of the exact prior form T-matrix

$$T_{fi} = \langle \chi_b^{(-)} \chi_x^{(-)} | U_{bx} | \Psi_a^{(+)} \rangle \quad (A.1)$$

the model can be derived by replacing the full solution $\Psi_a^{(+)}$ of the Hamiltonian of the system (with the incoming particle a) by plane waves

$$\Psi_a^{(+)} \approx e^{i\mathbf{p}_a \cdot \mathbf{r}_a / \hbar} \phi_{bx}(\mathbf{r}_b - \mathbf{r}_x) \quad (A.2)$$

and by rewriting the scattering waves $\chi_b^{(-)}$ and $\chi_x^{(-)}$ in terms of the off-shell t-matrices [11]

$$\chi^{(-)}(\mathbf{r}, \mathbf{p}) = e^{i\mathbf{p}\mathbf{r}/\hbar} + \frac{1}{(2\pi)^3} \int d^3p' \frac{t(\mathbf{p}', \mathbf{p}) e^{i\mathbf{p}'\mathbf{r}/\hbar}}{p'^2 - p^2 + i\epsilon} \quad (A.3)$$

In these expressions U_{bx} is the interaction between the cluster fragments b and x. It gives rise to the bound state of the projectile, represented by the ground state wave function $\phi_{bx}(\mathbf{r}_b - \mathbf{r}_x)$. The equations A.1 and A.3 allow to formulate the ('full finite range') T-matrix-element for the elastic break-up, say when x is the elastically scattered participant [11] by

$$T_x = - (2\pi)^{3/2} \frac{\hbar^2}{2m_x} t(\mathbf{p}_a - \mathbf{p}_b, \mathbf{p}_x) \cdot \tilde{\Phi}\left(\frac{m_b}{m_a} \mathbf{p}_a - \mathbf{p}_b\right) \quad (A.4)$$

with $\tilde{\Phi}(\mathbf{p}_{b0} - \mathbf{p}_b)$ being the Fourier transformed bound state wave function. Thus, apart from a phase space factor $\rho(E_b, \Omega_b)$, the elastic break-up cross section for finding the fragment b with \mathbf{p}_b

$$\frac{d^4\sigma}{d\Omega_b dE_b d\Omega_x dE_x} = \frac{d^2\sigma^{(xA)}}{d\Omega_x dE_x} |\tilde{\Phi}(\mathbf{q})|^2 \rho(E_b, \Omega_b) \quad (\text{A.5})$$

is essentially given by the cross section for the elastic scattering of the participant x which has dissociated with the momentum $\mathbf{p}_a - \mathbf{p}_b$ and scattered with \mathbf{p}_x , multiplied by the probability of finding the momentum $\mathbf{q}_b = (m_b/m_a) \mathbf{p}_a - \mathbf{p}_b = \mathbf{p}_{b0} - \mathbf{p}_b$ in the momentum distribution of the cluster motion.

The comparison with inclusive type measurements requires a summation over the unobserved reaction channels of the participant, so that the double differential cross section may be written as

$$\frac{d^2\sigma}{d\Omega_b dE_b} = \tilde{\sigma}_{xA} \cdot |\tilde{\Phi}(\mathbf{q})|^2 \cdot \rho(E_b, \Omega_b) \quad (\text{A.6})$$

with $\tilde{\sigma}_{xA}$ being modified (due to the presence of the spectator) total cross section for the participant-target interaction (see [33-35]). The simplification introduced by the Serber model is based on a geometrical approximation for the absolute value of the cross section, thus ignoring a possible dependence of $\tilde{\sigma}_{xA}$ on \mathbf{p}_b . Actually, approximating $\tilde{\sigma}_{xA}$ by the total reaction cross section σ_{xA} of a 'projectile x' colliding with the target A, optical model calculations using the potential parameters given in [36] show that the geometrical estimate is a rather good approximation. A more serious type of distortions results from the influence of the target field on the motion of the spectator particle.

In order to account at least for effects due to the long-range Coulomb field, one may introduce into the QFBM approach Coulomb waves instead of plane waves for the projectile and ejectile motion [33-35]. It has been shown by McVoy and Nemes [37] that in the semi-classical region, where the contribution of far side running waves can be neglected, the Coulomb scattering waves can be approximated by plane waves with a local Coulomb corrected momentum \mathbf{p}' . It is determined by

$$p'^2 = p^2 - 2m Z_T Z e^2 / R \quad (\text{A.7})$$

and

$$\frac{\mathbf{p} \cdot \mathbf{p}'}{p p'} = \cos\left(\tan^{-1} \frac{\eta}{l}\right) \quad (\text{A.8})$$

Here \mathbf{p} is the asymptotic momentum, Z_T the charge of the target, R the distance of closest approach for the projectile with mass m and charge Z , η is the Sommerfeld parameter and ℓ is the orbital angular momentum corresponding to R .

Thus the difference of the asymptotic momenta

$$|\mathbf{p}_{b0} - \mathbf{p}_b| = |\mathbf{q} + \mathbf{d}_a + \mathbf{d}_b| \quad (\text{A.9})$$

displays the internal momentum of the fragment b in the projectile with a rotation by \mathbf{d}_a (of the projectile motion) and \mathbf{d}_b (of the ejectile motion). Assuming that the break-up reactions take place in the region of the 'distance of closest approach' i.e. at a definite locus R the rotation can be calculated by eqs. A.7 and A.8.

Fig. 14 shows q as a function of the observed difference $|\mathbf{p}_{b0} - \mathbf{p}_b|$ for the case of break-up alpha particles observed at $\Theta_L = 15^\circ$ from the break-up of 156 MeV ${}^6\text{Li}$ -ions. The two

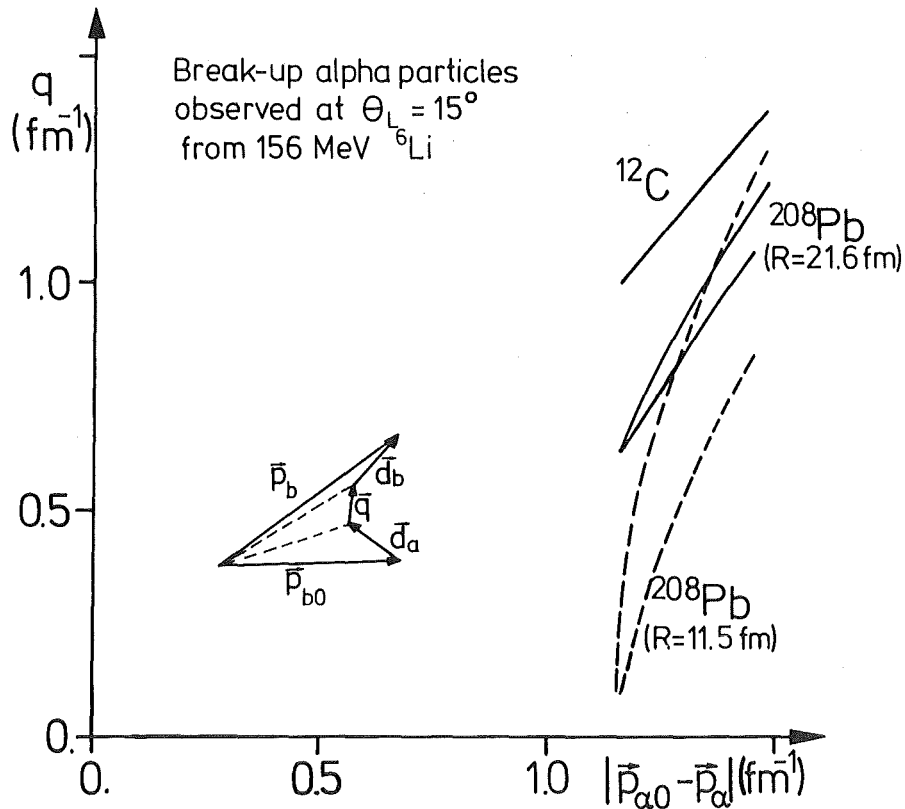


Fig. 14: Actual relative momentum q at the break-up point dependent on the difference of the asymptotic momenta.

branches correspond to ejectile energies smaller and larger than the beam velocity energy, respectively, i.e. to different relative directions of \mathbf{q} and $\mathbf{p}_{\alpha 0}$ with the same absolute value q . Obviously the Coulomb effects are negligible in the case of a ^{12}C -target and largely reduced when R is increased, which means large-impact parameter collisions.

In contrast to the Serber model with the extension, eqs. A.7 - A.9 include that the kinetic energy of the projectile at the point of break-up is dependent on R and that the Coulomb deflection is dependent on the ejectile energy. This might be the origin of some distortions if the condition $p_{b0} \gg q$ is not well met.

Strictly, in addition to the influence of the 'target' field, actually inducing the break-up, one has to consider the mutual interactions of the fragments in the final state (see angular distribution in Fig.11a above 3°). This type of distortion, dependent on the relative energy and well known in knock-out reactions, can hardly be specified in inclusive measurements where the participant interactions are not observed. The neglect of the final state interaction of the ejectiles is just typical for the simplification of the actual three-body problem by a spectator-participant approach.

Appendix B. Energy shifts of the break-up maxima

A peculiarity of the experimental data, which is not well reproduced within the Serber model, is the shift of the break-up maxima in the energy spectra from beam velocity energies to lower energies dependent on the observation angle. This feature has been already reported in ^6Li break-up studies with light targets [5], and it is generally observed for projectile-like reaction products in heavy ion collisions [38].

For determination of the shifts the physical background was subtracted before as described in chapter 4. This subtraction diminishes the shifts increasingly with increasing emission angle and is a small effect (for example 0.2 MeV at $\Theta = 6^\circ$ and 0.9 MeV at $\Theta = 12^\circ$, ^{12}C -target). The remaining shifts from the reaction $^{12}\text{C}(^6\text{Li},\alpha X)$ are shown in Fig. 15, obtained by least square fits* of Lorentzian curves to the experimental data, where the error bars represent the accuracy of these fits. (The parameters of the Lorentzian curves without background subtraction for the ^{12}C and the ^{208}Pb -target are tabulated in [18].) It should be noted that due to the finite accuracy of the energy calibration the measured shifts can vary together within a range of ± 300 keV, which does not yield a qualitative change.

The shifts cannot be understood in terms of the target recoil, target excitation or of the Q -value (1.47 MeV) of the ^6Li break-up reaction. An explanation within the frame of the

* We are indebted to Dipl. Phys. S. Göring for calculating these parameter fits.

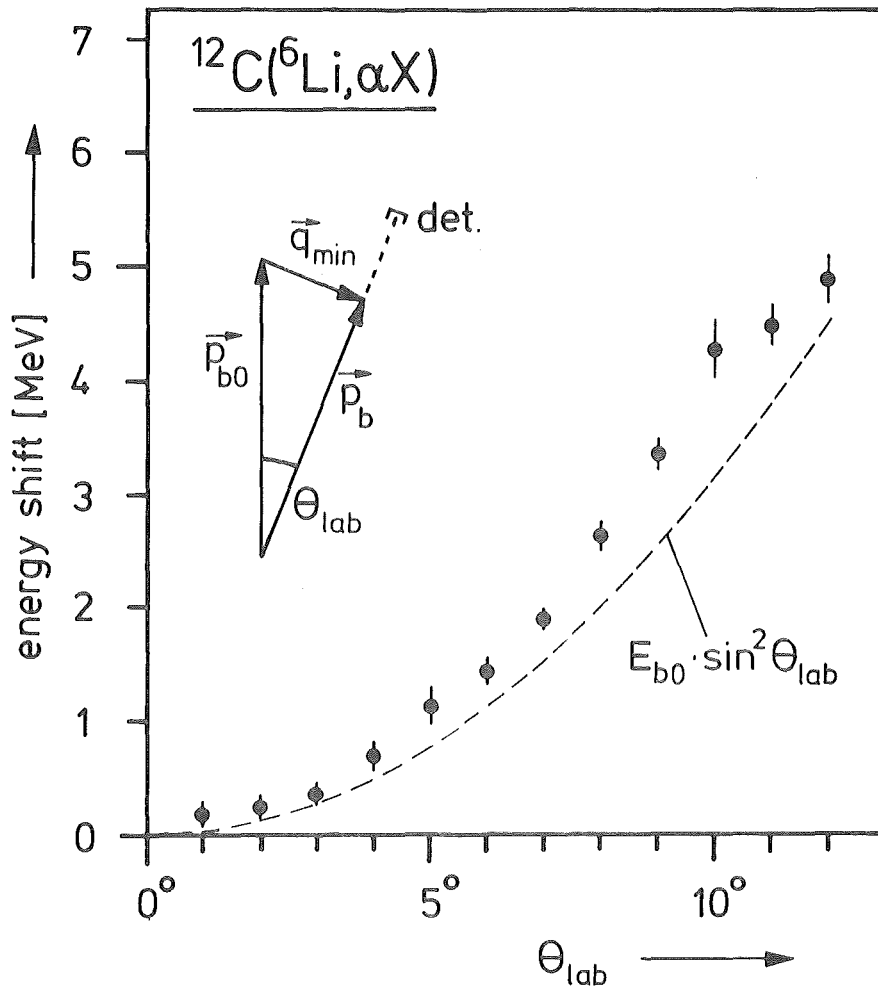


Fig. 15: Shifts of the break-up maxima in the inclusive alpha particle spectra with respect to the beam velocity energy E_{b0} ($= 103.5$ MeV corrected for the energy loss in the target). The inset indicates a tentative explanation in the case where Coulomb effects may be ignored.

spectator mechanism is of geometrical type. When neglecting the Coulomb deflection, which is reasonable for ^{12}C , the minimum relative momentum for the α -d-motion at a fixed observation angle is given at a laboratory momentum $p_b = p_{b0} \cos \theta_{\text{lab}}$ (see momentum vectors in Fig. 15) and having the largest probability it defines the maximum of the energy spectrum. It follows that the maximum is shifted from the beam velocity energy to lower energies by a value of $E_{b0} \sin^2 \theta_{\text{lab}}$, represented by the dashed line in Fig. 15. The agreement with the measured shifts is satisfactory and is even not much affected when leaving out

the background correction. Also the phase space factor (eq. 5.1), which causes a slight shift to larger energies equally for all observation angles, does not yield a significant change. As a consequence the energies due to the Q-value of ${}^6\text{Li}$ break-up and due to recoil effects are given by the participant x.

In the ${}^{208}\text{Pb}$ case the constant energy shift of the alpha particle spectra below 8° can be partly understood, considering the superposition of contributions from different Coulomb deflection angles, simply as an average shift resulting from this geometric effect. Calculations correcting this effect within the extended spectator model show that the calculated spectra for ${}^{208}\text{Pb}$ are shifted to lower energies by 0.5 MeV to 1 MeV so that a shift of about 1 MeV still remains.

References

- [1] Budzanowski,A. in "Dynamics of Heavy-Ion Collisions", Proc. 3rd Adriatic Europhysics Conf., Hvar, Yugoslavia, 25 - 31 May 1981, p. 189, eds. Cindro,N., Ricci,R.A., Greiner,W., North Holland - Amsterdam - New York - Oxford (1981)
- [2] Castaneda,C.M., Smith Jr.,H.A., Singh, P.P., Karwowski,H.: Phys. Rev. C21, 179 (1980)
- [3] Neumann,B., Buschmann,J., Klewe-Nebenius,H., Rebel,H., Gils,H.J.: Nucl. Phys. A329, 259 (1979)
- [4] Neumann,B., Rebel,H., Buschmann,J., Gils,H.J., Klewe-Nebenius,H., Zagromski,S.: Z. Physik A296, 113 (1980)
- [5] Neumann,B., Rebel,H., Gils,H.J., Planeta,R., Buschmann,J., Klewe-Nebenius,H., Zagromski,S., Shyam,R., Machner,H.: Nucl. Phys. A382, 296 (1982)
- [6] Rebel,H. in "Nuclear Collective Dynamics", Lectures of the 1982 Int. Summer School of Nucl. Phys., Poiana Brasov, Romania, 26.8.- 7.9.1982, p.432, eds. Bucurescu,D. Zamfir,N.F., World Scientific Publ., Singapore (1983)
- [7] Shotter,A.C. in "Clustering Aspects of Nuclear Structure", Proc. 4th Int. Conf. on Clustering Aspects of Nuclear Structure and Nuclear Reactions, Chester, U.K., 23-27 July 1984, p.199, eds. Lilley,J.S., Nagarajan,M.A., Reidel,D., Publ. Comp. Dordrecht - Boston - Lancaster (1985)
- [8] Serber,R.: Phys. Rev. 72, 1008 (1947)
- [9] McVoy,K.W. in "Coincident Particle Emission from Continuum States in Nuclei", Proc. Bad Honnef, 4-7 June 1984, p.484, eds. Machner,H., Jahn,P., World Scientific Publ., Singapore (1984)
Hussein,M.S., McVoy,K.W.: Nucl. Phys. A445, 124 (1985)
- [10] Shyam,R., Baur,G., Rösel,F., Trautmann,D.: Phys. Rev. C22, 1401 (1980)
- [11] Baur,G., Rösel,F., Trautmann,D., Shyam,R.: Phys. Rep. (Phys. Lett. C) 111, 333 (1984)
- [12] Ehret,H.P., Ernst,R., Friedrich,L., Hurst,A., Huttel,E., Kaltenbaek,J., Schulz,F., Wiss,L., Ziegler,P.: KfK-Report 4159, p. 194, eds. Büche,G., Doll,P., Friedrich,L., Kernforschungszentrum Karlsruhe (1986)
- [13] Bechtold,V., Friedrich,L., Schulz,F. in "10th Int. Conf. on Cyclotrons and their Appl.", East Lansing, Mich., 30.4.-3.5.1984
- [14] Gils,H.J.: KfK-Report 2972, Kernforschungszentrum Karlsruhe (1980)
- [15] Gils,H.J., Buschmann,J., Zagromski,S., Krisch,J., Rebel,H.: Nucl. Instr. Meth. (in press)

- [16] Gils,H.J., Jelitto,H., Schlösser,H., Zagromski,S., Buschmann,J., Eyrich,W., Hofmann,A., Kiener,J., Lehmann,A., Rebel,H.: Nucl. Instr. Meth. (in press)
- [17] Lehmann,A.: diploma thesis, Univ. Erlangen-Nürnberg (1987) (unpublished)
- [18] Jelitto,H.: Ph.D. thesis, Univ. Heidelberg (1987), KfK-Report 4259, Kernforschungszentrum Karlsruhe (1987)
- [19] Schlösser,H.: Ph.D. thesis, Univ. Erlangen-Nürnberg (1987)
- [20] Kozik,T., Buschmann,J., Neudold,M.: KfK-Report 3988B, Kernforschungszentrum Karlsruhe (1985)
- [21] Neumann,B.: Ph.D. thesis, Univ. Heidelberg (1979), KfK-Report 2887, Kernforschungszentrum Karlsruhe (1979)
- [22] Cook,J., Gils,H.J., Rebel,H., Majka,Z., Klewe-Nebenius,H.: Nucl. Phys. **A388**, 173 (1982)
- [23] Utsunomiya,H.: Phys. Rev. **C30** 1748 (1984)
- [24] Kukulín,V.I., Krasnopol'ski,V.M., Voronchev,V.T., Sazanov,P.B.: Nucl. Phys. **A417**, 128 (1984)
- [25] Utsunomiya,H., Kubono,S., Tanaka,M.H., Sugitani,M., Morita,K., Nomura,T., Hamajima,Y.: Phys. Rev. **C28** 1975 (1983)
- [26] Albinska,M., Albinski,J., Buschmann,J., Gils,H.J., Klewe-Nebenius,H., Rebel,H., Zagromski,S. in "Coincident Particle Emission from Continuum States in Nuclei", Proc. Bad Honnef, 4-7 June 1984, p. 326, eds. Machner,H., Jahn,P., World Scientific Publ., Singapore (1984)
- [27] Schaller,L.A., Schellenberg,L., Phan,T.Q., Piller,G., Ruetschi,A., Schneuwly,H.: Nucl. Phys. **A379** 523 (1982)
- [28] Euteneuer,H., Friedrich,J., Voegler,N.: Nucl. Phys. **A298** 452 (1978)
- [29] Akhieser,A.I., Sitenko,A.G.: Phys. Rev. **106** 1236 (1957)
- [30] Lovas,R.G., Kruppa,A.T., Beck,R., Dickmann,F.: Nucl. Phys. **A474**, 451 (1987)
- [31] Ent,R., Block,H.P., van Hienen,J.F.A., van der Steenhoven,G., van den Brand,J.F.J., den Herder,J.W.A., Jans,E., Keizer,P.H.M., Lapikas,L., Quint,E.N.M., de Witt Huberts,P.K.A., Berman,B.L., Briscoe,W.J., Christou,C.T., Lehman,D.R., Norum,B.E., Saha,A.: Phys. Rev. Lett. **57** 2367 (1986)
- [32] Clement,H. in "Advanced Methods in the Evaluation of Nuclear Scattering Data", eds. Krappe,H.,J., Lipperheide,R., Lecture Notes in Physics **236** p. 324, Springer-Verlag, Berlin - Heidelberg - New York - Tokyo (1985)
- [33] Aarts,E.H.L., Malfliet,R.A.R.L., van der Werf,S.Y., de Meijer,R.J.: Nucl. Phys. **A380**, 23 (1982)
- [34] Aarts,E.H.L., Malfliet,R.A.R.L., de Meijer,R.J., van der Werf,S.Y.: Nucl. Phys. **A425**, 23 (1984)

- [35] Aarts,E.H.L., Malfliet,R.A.R.L., de Meijer,R.J., van der Werf,S.Y.,
Baur,G., Shyam,R., Rösler,F., Trautmann,D.: Nucl. Phys. **A439**, 45 (1985)
- [36] Nolte,M., Machner,H., Bojowald,J.: Phys. Rev. **C36** 1312 (1987)
Machner,H. (private communications)
- [37] McVoy,K.W., Nemes,M.C.: Z. Phys. **A295**, 177 (1980)
- [38] Siemssen,R.H. in "Heavy Ions and Nuclear Structure", Nucl. Science
and Research Conf. Series Vol. 5, p. 1, eds. Sikora,B., Wilhelmi,Z.,
Harwood Academic Publ., London (1984),